Detection of trapped molecular O_2 in a charged Li-rich cathode by Neutron PDF

Robert A. House[1,2,3], Helen Y. Playford[4], Ronald I. Smith[4], Jennifer Holter[1], Ian Griffiths[1], Ke-Jin Zhou[5], Peter G. Bruce[1,2,3,6,*]

1. Department of Materials, University of Oxford, Parks Road, Oxford, OX1 3PH, U.K.
2. The Henry Royce Institute, Parks Road, Oxford, OX1 3PH, UK
3. The Faraday Institution, Quad One, Becquerel Avenue, Harwell Campus, Didcot, OX11 0RA, UK
4. ISIS Neutron and Muon Source, Rutherford Appleton Laboratory, Harwell Campus, Didcot, OX11 0QX, UK
5. Diamond Light Source, Harwell Campus, Didcot, UK
6. Department of Chemistry, University of Oxford, South Parks Road, Oxford, OX1 3QZ, U.K.

* Corresponding Author: peter.bruce@materials.ox.ac.uk

Abstract

Oxidation and reduction of the oxide ions in the bulk of cathode materials is a potential route towards increasing the energy density of Li-ion batteries. Here, we present neutron PDF data which demonstrates the presence of short 1.2 Å O-O distances in a charged O-redox cathode material, corresponding to the bond length of molecular O_2. This was achieved by collecting our data close to absolute zero (2K), suppressing thermal motion which may have obscured detection by PDF previously. This direct detection of molecular O_2 trapped in the material by diffraction complements the X-ray spectroscopy studies by e.g. RIXS while avoiding issues of possible beam damage as well as being a bulk average technique.

Broader Context

Lithium-rich cathode materials, such as $Li_{1.2}Ni_{0.13}Co_{0.13}Mn_{0.54}O_2$, represent a potential route towards the important goal of increasing the energy density of Li-ion batteries, important for applications in EVs, aviation and portable electronics. They are able to store more charge than conventional cathode materials through redox chemistry involving the oxide ions in the structure, but they suffer from voltage and capacity loss as a result. Characterising the nature of oxidised oxygen and tying it to the structural changes in these materials has attracted a considerable research effort. Here, we interrogate the local atomic structure of charged $Li_{1.2}Ni_{0.13}Co_{0.13}Mn_{0.54}O_2$ electrodes by employing neutron total scattering on ^{7}Li-enriched material at temperatures close to absolute zero (2K), to reduce the influence of background absorption and thermal motion. Under these measurement conditions, we report the first direct structural evidence for the existence of O_2 molecules trapped within the cathode structure and identify nickel as the species responsible for out-of-plane migration. With this understanding, we demonstrate that uniform, spherical cathode particles which exhibit less surface O_2 loss and more trapped O_2, show greater coulombic efficiencies as a result, pointing a way towards higher performance materials.

Introduction

Cathode materials that can store charge more densely and at higher average voltages are required for next generation Li-ion batteries with higher energy densities.[1] Existing cathodes operate through oxidation and reduction of the transition metal ions. Extending the redox chemistry onto the oxide ions (O-redox) is a potential route to higher energy density, however, O-redox is accompanied by

complex structural changes that must be fully understood as they lead, among other things, to voltage hysteresis (loss).[2–8] In particular, identifying the species of oxidised O present in O-redox cathodes has proved to be a significant challenge. Early studies in the field proposed O oxidation involved formation of long O-O dimers and peroxides.[8–10] Recently, spectroscopic methods, in particular high-resolution RIXS, have pointed towards the existence of O_2 molecules trapped inside the bulk particles of O-redox cathodes.[11–13]

Diffraction studies have so far been unable to evidence any type of bonded O-O species in charged O-redox cathodes. Bragg diffraction is not sensitive to localised defects, although some reports have been made of an increased number of oxide vacancies in the lattice during charge.[3,14–16] Pair distribution function (PDF) analysis of total scattering data offers access to information about the short range structure, however it has proved difficult to collect data that can unambiguously reveal peaks at very low interatomic distances (< 1.5 Å); the O-O distance in O_2 is 1.2 Å.[17–22]

Here, we present neutron PDF data which reveal the presence of short 1.2 Å O-O bonds in charged $Li_{1.2}Ni_{0.13}Co_{0.13}Mn_{0.54}O_2$, providing the first direct structural evidence for molecular O_2 trapped in the bulk. We overcome experimental challenges that may have previously obscured the observation of O_2 molecules with PDF techniques, by measuring large sample volumes of 100% ^{7}Li-enriched material at temperatures close to absolute zero (2K). This reduces significantly the background absorption and thermal motion, enabling detection of the molecular species present. Through fitting the PDF, we estimate approx. 20% of the O atoms are present in the form of O_2, which is broadly in agreement with the amount expected from the charge passed from O oxidation (16%) after accounting for the amount of O_2 evolved. We also show that smaller particles lead to somewhat less trapped O_2 and more O_2 evolved, in accord with an overall lower cycling efficiency, highlighting the importance of morphological control in promoting formation of O_2 in the bulk, rather than at the surface.

Results and Discussion

The Pristine Structure

A 10g batch of 100% ^{7}Li-enriched $Li_{1.2}Ni_{0.13}Co_{0.13}Mn_{0.54}O_2$ was prepared by carbonate co-precipitation, as detailed in Methods, for the neutron study. $Li_{1.2}Ni_{0.13}Co_{0.13}Mn_{0.54}O_2$ was also prepared by sol-gel for the comparison study which we return to later. Powder X-ray diffraction (PXRD) data confirmed a single-phase product was obtained with the characteristic honeycomb superstructure peaks, Supplementary Figure 1. Homogeneous mixing of the transition metal (TM) ions within and between the primary particles was verified with energy dispersive X-ray (EDX) analysis, Supplementary Figure 2. The electrochemical load curve for the first cycle is shown in Figure 1a. The material exhibits a discharge capacity of 300 mAh g^{-1} at an average voltage of 3.5 V and a first cycle coulombic efficiency of 85%, in line with other reports on Li-rich NMC prepared by co-precipitation.[18,23,24]

Neutron total scattering data were collected on $^7Li_{1.2}Ni_{0.13}Co_{0.13}Mn_{0.54}O_2$ at room temperature, see Methods for details. The atomic pair distribution function (PDF) was fitted between 0.5 – 40 Å to a C2/m structural model with honeycomb ordering within the TM layer and without TM ions in the Li layer, Figure 1b. As shown in Figure 1c, a close fit to the data is obtained over both the short (0-10 Å) and medium range (10-40 Å) length-scales confirming the site preferences of Li/Ni and Co/Mn in the 2b and 4g Wycoff positions respectively. Unlike with X-rays, Ni, Co and Mn can all be clearly distinguished in neutron diffraction due to differences in their scattering lengths (Ni = 10.3 fm, Co = 2.49 fm and Mn = -3.73 fm).

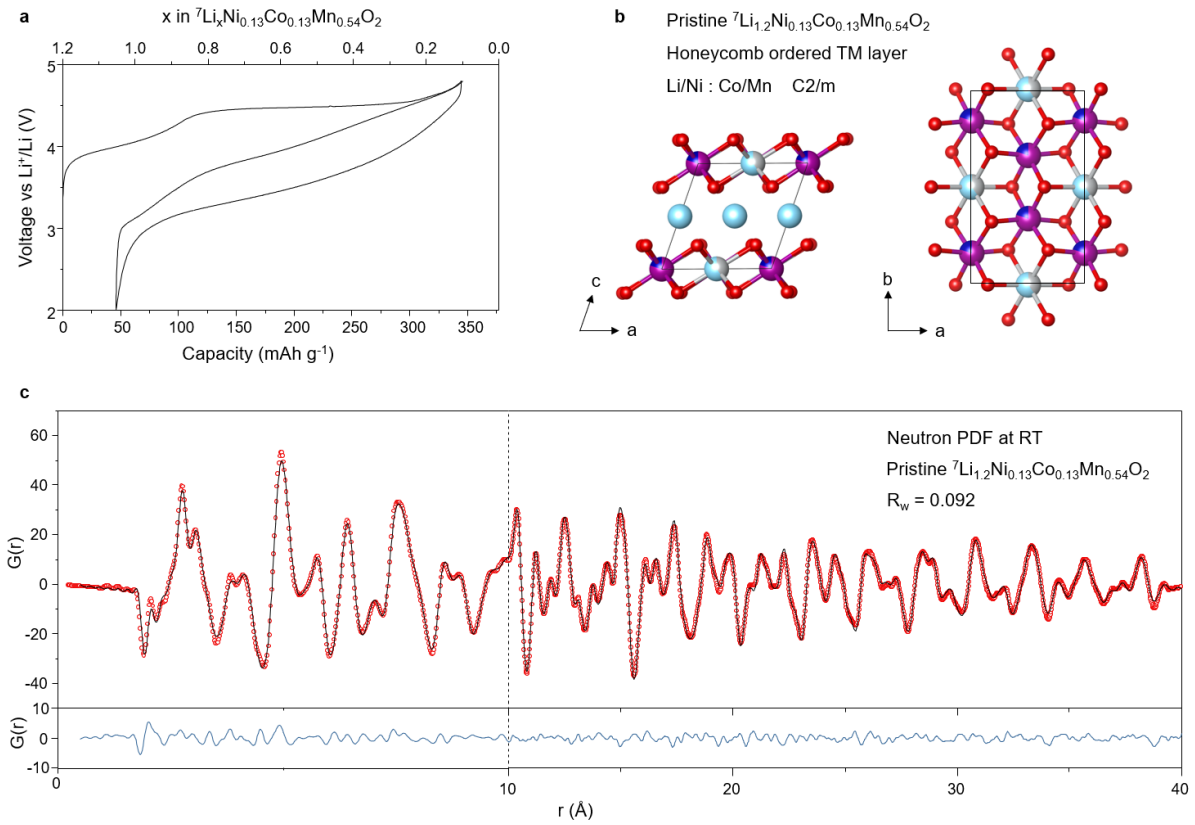

Fig. 1. Electrochemistry, Structure and Neutron PDF of pristine $^7Li_{1.2}Ni_{0.13}Co_{0.13}Mn_{0.54}O_2$. a Electrochemical load curve for $^7Li_{1.2}Ni_{0.13}Co_{0.13}Mn_{0.54}O_2$ cycled between 2 - 4.8V at 20 mA g^{-1}. **b** Refined structural model from neutron PDF data using C2/m space group with honeycomb ordering of Li/Ni and Co/Mn: pale blue, Li; grey, Ni; dark blue, Co; purple, Mn. **c** Neutron PDF for $^7Li_{1.2}Ni_{0.13}Co_{0.13}Mn_{0.54}O_2$ generated from total scattering data collected at room temperature, Q_{max} = 30 Å.

The Charged Structure

On the first charge, $Li_{1.2}Ni_{0.13}Co_{0.13}Mn_{0.54}O_2$ exhibits a long voltage plateau at 4.5 V during which O oxidation occurs. Extensive studies have been performed to investigate the structural changes taking place during this plateau. It is now understood that the honeycomb ordered arrangement of Li and TM ions in the TM layer is irreversibly lost due to in-plane and out-of-plane TM migration.[2,12,24–27] However, there remains ambiguity around the identity of the migrated TM ions, oxidised O species and the nature of the local structure of the material in the bulk.

To investigate the structure of the charged phase in depth, X-ray diffraction and neutron total scattering data for PDF analysis, were collected for $^7Li_{1.2}Ni_{0.13}Co_{0.13}Mn_{0.54}O_2$ charged to 4.8V. As shown in Figure 2a, the long range structure of $^7Li_{0.1}Ni_{0.13}Co_{0.13}Mn_{0.54}O_2$ conforms to a single phase and can be fitted well to a C2/m structural model without honeycomb ordering, Figure 2b. The lack of superstructure peaks in the charged phase is in accord with loss of in-plane honeycomb ordering in line with previous studies.[2,12,24–27] The out-of-plane TM migration was also refined using these data giving an occupancy value of 0.03 TM ions in the Li layer (i.e. 3%) however, since the X-ray scattering factors of Mn, Co and Ni are too similar to distinguish by PXRD, X-rays alone cannot identify which element is responsible for the anti-site defects.

The C2/m structural model was also refined against the neutron PDF data, at first without out-of-plane migration, Figure 2c. A close fit to the data can be obtained, except for some local structural features

in the region below around 4-5 Å, indicating this model offers a good average description for the medium-range structure.

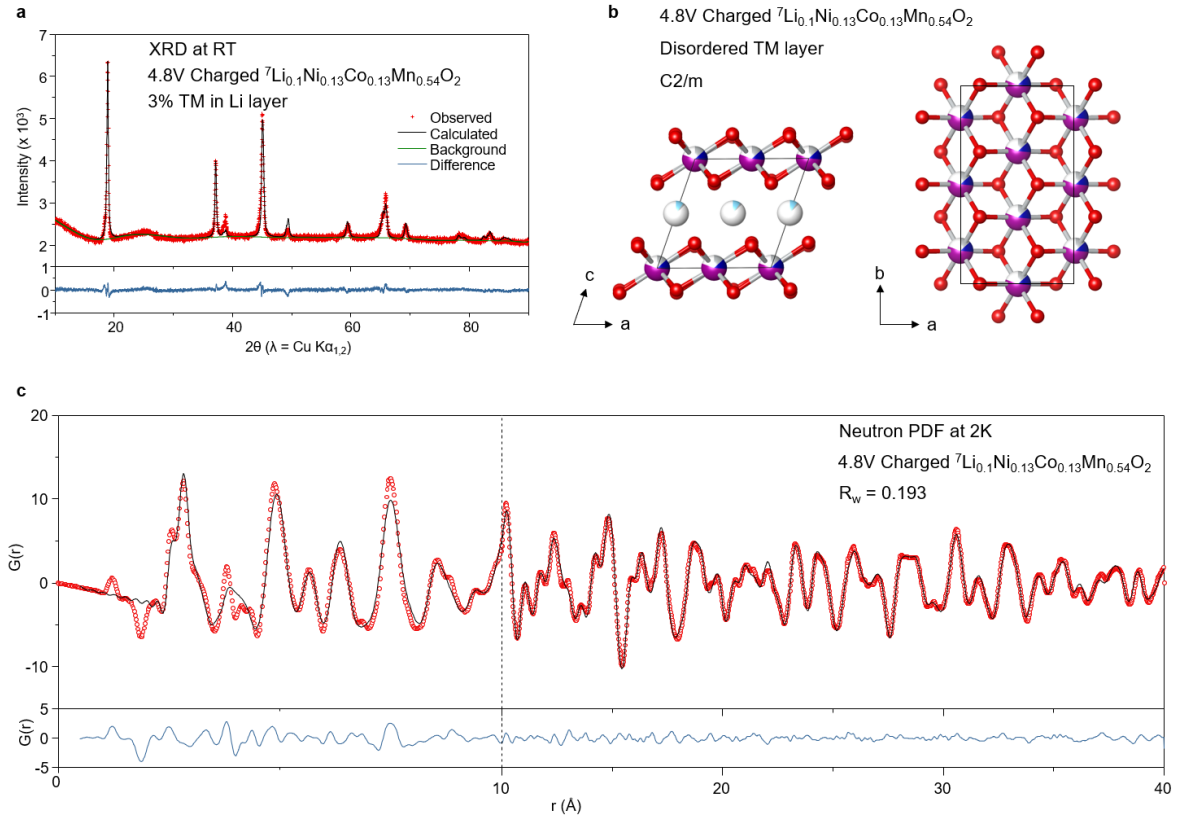

Fig. 2. PXRD data, Structure and Neutron PDF of $^7Li_{1.2}Ni_{0.13}Co_{0.13}Mn_{0.54}O_2$ charged to 4.8V. a Rietveld refinement of powder X-ray diffraction data of $^7Li_{0.1}Ni_{0.13}Co_{0.13}Mn_{0.54}O_2$ using a C2/m space group. No superstructure peaks are observed indicating there is no in-plane ordering of Ni/Mn/Co. Refinements showed 0.03 occupancy of Li layer sites by TM (i.e. 3% occupancy), however Ni, Co and Mn are indistinguishable with X-rays. **b** Refined structural model from neutron PDF data using C2/m space group with no in-plane ordering of Ni/Mn/Co and no out-of-plane TM migration: pale blue, Li; grey, Ni; dark blue, Co; purple, Mn. **c** Neutron PDF data for $^7Li_{0.1}Ni_{0.13}Co_{0.13}Mn_{0.54}O_2$ generated from total scattering data collected at 2K, Q_{max} = 26 Å.

To investigate the local structure focussing on the shorter length scale in order to probe any O-O species, further fittings were performed in the range 0.5 - 4 Å, Figure 3a. An improved fit is observed, in particular, the peaks at 2.6 Å and 3.8 Å, indicating a slight deviation in the local and average structures due to the presence of localised defects or distortions, however the fit to the trough at 1.86 Å and peak at 2.23 Å remain relatively poor. Peaks in the PDF correspond to interatomic distances and from the interatomic distances anticipated from the structural model, Figure 3c, it is clear these two peaks arise from TM-O pairs in the TM and Li layers respectively. In PDF, peaks arise when the product of the scattering lengths of atom-atom pairs is positive and troughs when negative. Since O has a positive scattering length (5.80 fm), this implies that the model contains too many TM ions with positive scattering lengths in the TM layer and too few in the Li layer to account for the data. Ni has the strongest positive scattering length (10.3 fm), almost four times that of Co. A further refinement was performed allowing for Ni to vary between the TM and Li layers. The best fit was obtained with an occupancy of 0.03 Ni in the Li layer, in line with the occupancy of the Li sites in the Li layer by TM ions determined by PXRD. Thanks to the much greater difference in scattering length between Mn, Co

and Ni with neutrons (Mn = -3.73 fm, Co = 2.49 fm, Ni = 10.3 fm) than X-rays, we are therefore able to conclude that Ni is the primary TM ion responsible for the out-of-plane migration observed in Li-rich NMC.

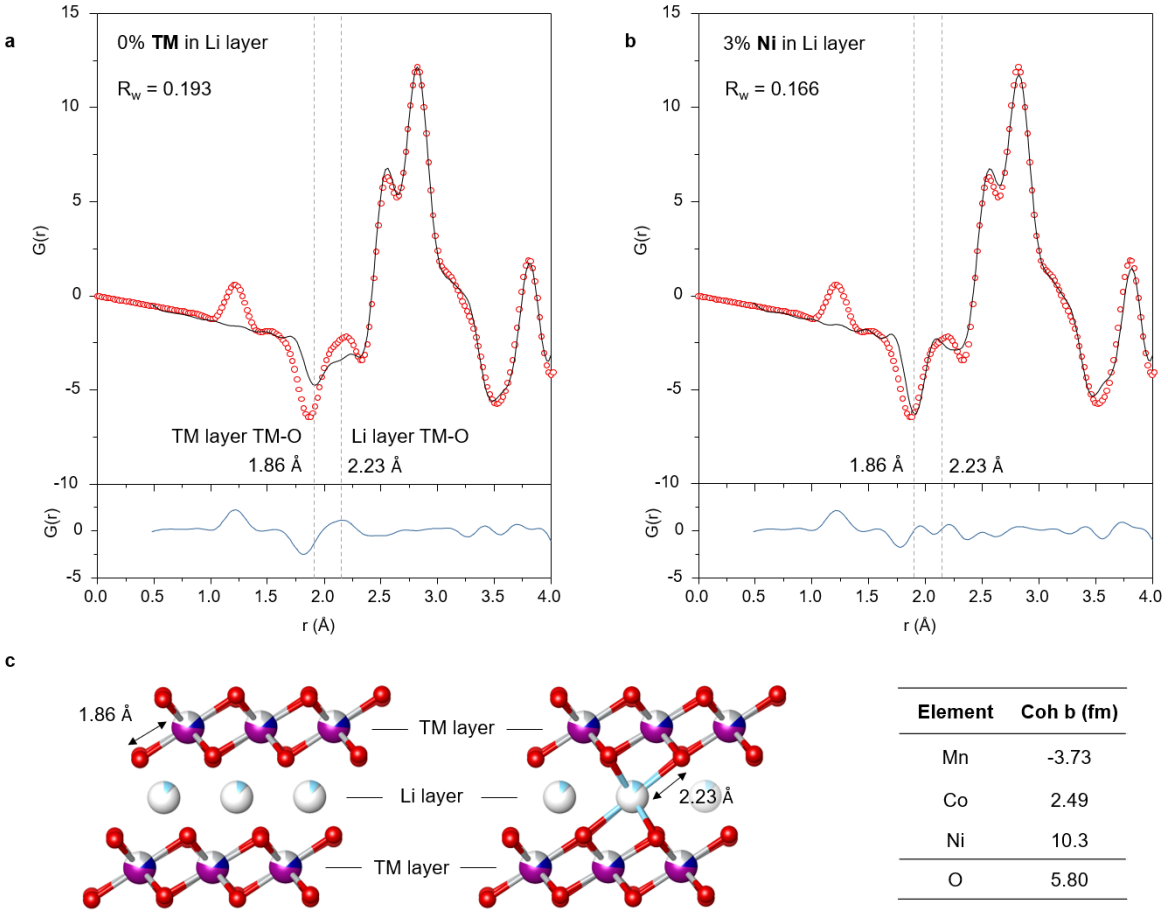

Element	Coh b (fm)
Mn	-3.73
Co	2.49
Ni	10.3
O	5.80

Fig. 3. Out-of-plane Ni migration from Neutron PDF. a Neutron PDF in 0.5 – 4 Å region fitted without TM migration. **b** Neutron PDF in 0.5 – 4 Å region fitted allowing out-of-plane Ni migration. An occupancy value of 0.03 (i.e. 3%) is obtained. **c** Structural models showing TM-O bond length in TM layer and in Li layer. Ni, Mn and Co can be readily distinguished by neutrons thanks to sizeable differences in their scattering lengths (coh b).

<u>The peak at 1.2 Å</u>

Detecting molecular species with such short atom-atom pair lengths as 1.2 Å is a significant challenge for PDF, requiring long collection times for good signal-to-noise at high Q. Furthermore, molecular species which are only weakly bound within nanovoids in the material will be much more mobile than atoms which are chemically bound within a crystal lattice, given available thermal energy, reducing the strength of the observable interatomic correlations.

The data presented here, Figure 4a, show the first clear evidence from PDF of a detectable 1.2 Å peak in charged Li-rich NMC corresponding to the O-O bond in molecular O_2. To overcome the challenges, the data were collected with the sample cooled to 2K in a cryostat to limit the influence of thermal motion. The neutron PDF data were obtained by using a large sample volume and reducing the sources of absorption significantly, through 100% ^{7}Li enrichment. The use of neutrons provides not only bulk average structural information but is also free from possible beam damage effects, a common concern

with X-ray or electron spectroscopies. Neutron PDF is capable of distinguishing between different O-O species with different bonds. No evidence was observed for peroxide or superoxide.

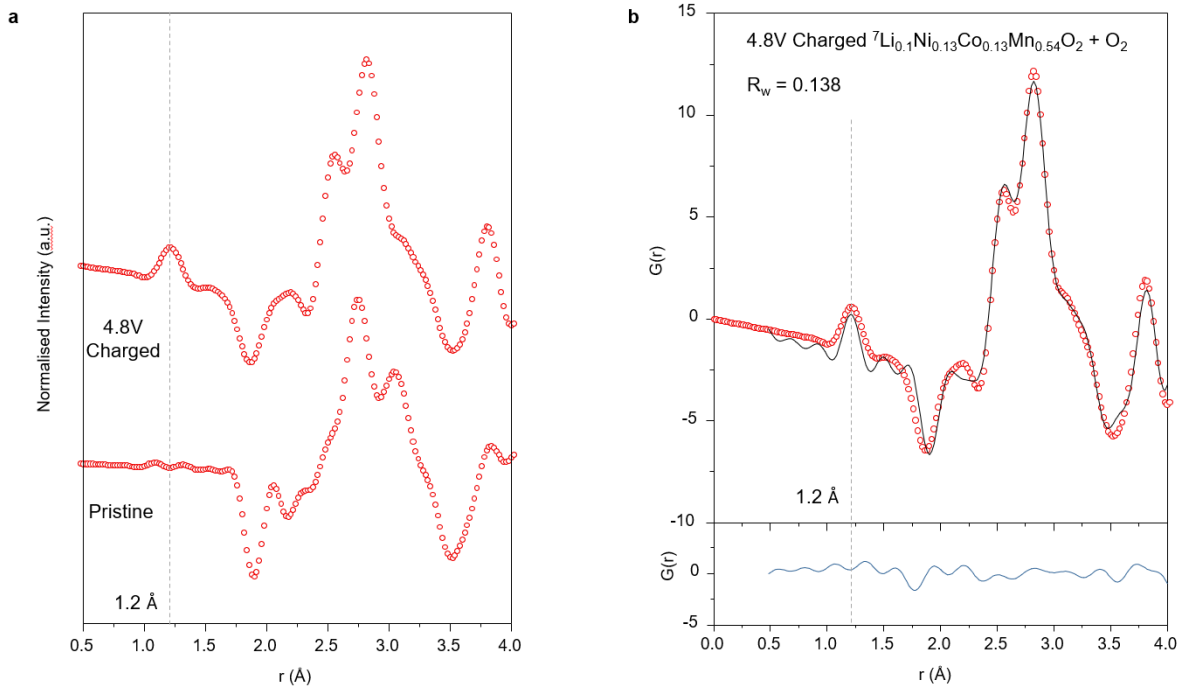

Fig. 4. 1.2 Å O-O bonds detected and quantified from Neutron PDF. a Neutron PDF of pristine $^7Li_{1.2}Ni_{0.13}Co_{0.13}Mn_{0.54}O_2$ and 4.8V charged $^7Li_{0.1}Ni_{0.13}Co_{0.13}Mn_{0.54}O_2$ highlighting the peak 1.2 Å corresponding to molecular O_2 (bond length 1.2 Å). There are no peaks corresponding to superoxide O_2^- (1.34 Å) or peroxide O_2^{2-} (1.49 Å) **b** Neutron PDF in 0.5 – 4 Å region fitted with 2 phases: $^7Li_{0.1}Ni_{0.13}Co_{0.13}Mn_{0.54}O_2$ and solid beta-O_2. Refined phase fractions indicate 20% of the O atoms are in the form of O_2.

The charged cathode material was dried under vacuum at room temperature before cooling to collect the NPDF data. The O_2 detected at low temperature reflects the O_2 trapped in the particles at room temperature. Furthermore, we have previously investigated the effect of temperature on trapped O_2 using high resolution RIXS and have shown there is no significant difference between the O_2 measured at room and very low temperatures.[12]

To obtain an estimate from the PDF data for the amount of molecular O_2 present in the material, a 2-phase refinement was performed with $^7Li_{0.1}Ni_{0.13}Co_{0.13}Mn_{0.54}O_2$ and solid O_2. Since there is little evidence of any intermolecular correlations between O_2 molecules in the PDF data, as evidenced by the quality of fit above 1.5 Å with just the $^7Li_{0.1}Ni_{0.13}Co_{0.13}Mn_{0.54}O_2$ model in Figure 3b, the solid O_2 was modelled as individual molecules by modifying the calculated PDF with a spherical shape function, effectively creating spherical nanoparticles with radii comparable to the intermolecular distance (i.e. containing only a single O_2 molecule) allowing only the peak at 1.2 Å to be fitted. From the results of the 2-phase refinement, we estimate that around 20% of the O atoms in the structure are in the form of O_2 molecules. This is in good agreement with the charge passed which implies 16% after accounting for the amount of O_2 evolved from the particles in charging as determined by operando mass spec, Supplementary Figure 3 (0.7 electrons p.f.u. O-redox capacity less the 0.08 electrons p.f.u. lost as O-loss gives 0.62 electrons p.f.u. which equates to 16% of the O^{2-} ions being oxidised to trapped O_2).

<u>$Li_{1.2}Ni_{0.13}Co_{0.13}Mn_{0.54}O_2$ synthesised by sol-gel and co-precipitation</u>

It is well established that synthesis conditions can have a significant impact on the performance of Li-rich NMC.[28–31] We have studied previously $Li_{1.2}Ni_{0.13}Co_{0.13}Mn_{0.54}O_2$ synthesised by sol-gel.[6,12] The 1st cycle load curves are compared in Fig. 5. The cycling efficiency of $Li_{1.2}Ni_{0.13}Co_{0.13}Mn_{0.54}O_2$ synthesised by co-precipitation and sol-gel methods is respectively 85 and 77%, in broad agreement with literature values.[18,23,24,32] In a recent paper, we proposed a general model for O-redox, in which oxidation of O^{2-} leads to O_2 that is either evolved from the particle surface or trapped in the bulk.[33] Comparing the SEM images for the materials synthesised by co-precipitation and sol-gel, Supplementary Figure 4, the former has a regular, compact and spherical secondary particle morphology whereas the morphology of the sol-gel material is more irregular and porous. Furthermore, as seen in the SEM, the primary particles of the sol-gel material are smaller than those prepared by co-precipitation. The greater surface to volume ratio for the sol-gel derived material is expected to lead to a higher proportion of O_2 lost from the particles and this is reflected in the differences between the ratio of O_2 lost:O_2 trapped for co-precipitation vs sol-gel, 1:8 and 1:3 respectively. The amount of O_2 trapped and lost in the case of the sol-gel material was reported by us previously.[6,12]

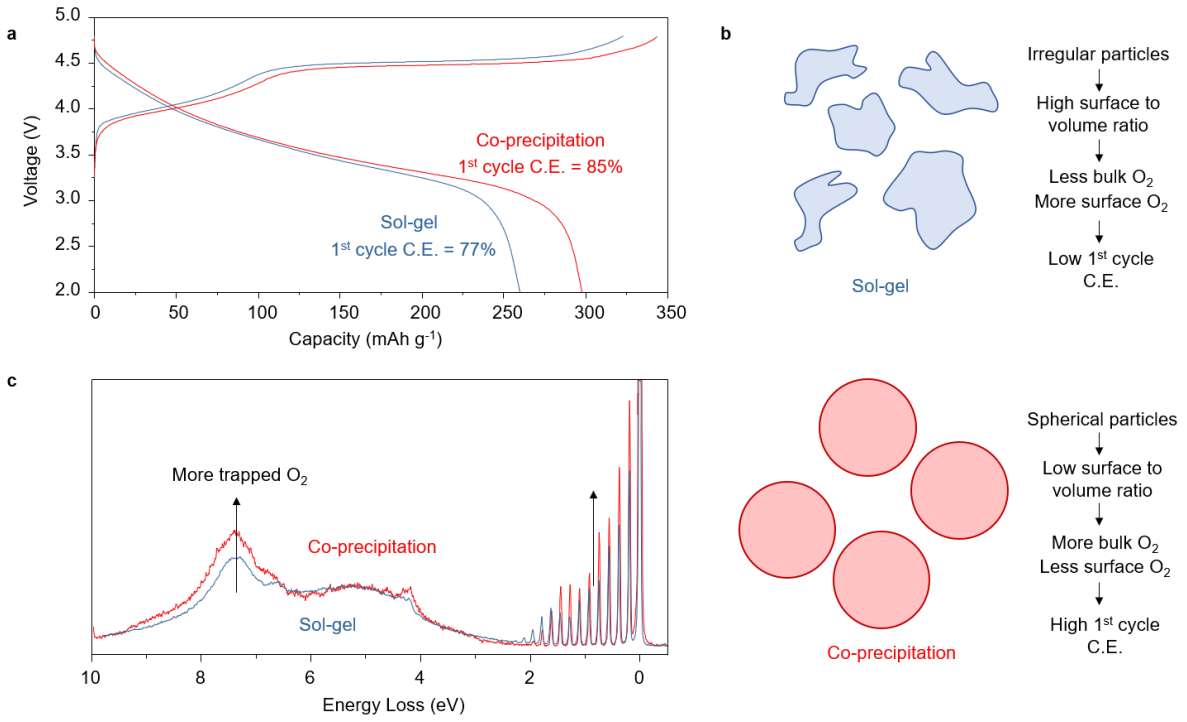

Fig. 5. Trapping more O_2 improves first cycle coulombic efficiency. a First cycle load curves and C.E.s for $Li_{1.2}Ni_{0.13}Co_{0.13}Mn_{0.54}O_2$ prepared by sol-gel and carbonate co-precipitation. **b** More regular secondary particle morphologies obtained from co-precipitation exhibit lower surface to volume ratios than sol-gel, SEM Supplementary Figure 4. and thus exhibit more trapped O_2 in the bulk. **c** RIXS measurements taken on both materials charged to 4.8V at 531 eV confirm more trapped O_2 in the high C.E. material prepared by co-precipitation.

To confirm this understanding, high resolution RIXS spectra were collected on each material in the fully charged state at 531 eV to probe the O_2 molecules that are trapped in the bulk. As shown in Figure 5c, there is an increase in the intensity of the energy loss features between 0-2 eV and at ~7.5 eV corresponding to molecular O_2 for the co-precipitation material, confirming the presence of a greater amount of trapped O_2 than in the sol-gel sample.

Conclusion

Here, we present neutron PDF results which provide the first direct structural evidence for the presence of trapped O_2 in Li-rich cathodes. The data clearly show a peak at 1.2 Å that can only be explained by molecular O_2, which we quantify as accounting for approx. 20 % of the O atoms in the cathode. The results complement spectroscopic data for trapped O_2, especially from RIXS, and serves to reinforce the role of trapped O_2 in the process of cycling Li-rich cathodes for Li-ion batteries.

Methods

Materials Preparation. A 10g batch of $^7Li_{1.2}Ni_{0.13}Co_{0.13}Mn_{0.54}O_2$ was prepared by carbonate co-precipitation. $Ni(NO_3)_2.6H_2O$, $Co(NO_3)_2.6H_2O$ and $Mn(NO_3)_2.4H_2O$ were dissolved in distilled water in a 1:1:4 molar ratio at a total concentration of 2 mol dm^{-3}. The nitrate solution was added dropwise along with a 2 mol dm^{-3} solution of Na_2CO_3 which was added in excess to a stirred RBF containing 100mL distilled water. The addition rate of each solution was controlled to maintain a pH of 7.8 throughout the reaction. The resulting suspension of mixed metal carbonate was left stirring overnight at 50°C after which it was filtered and washed with boiling distilled water to remove any unreacted Na_2CO_3. $^7LiOH.H_2O$ was prepared by reacting an appropriate amount of ^7Li metal (Cortecnet, 99.987 atom%) with distilled water. The solid, dried carbonate and lithium precursors were intimately ground together and heated to 500°C for 5 hours followed by 850°C for 15 hours using a ramp rate of 5°C min^{-1}. Sol-gel synthesised $Li_{1.2}Ni_{0.13}Co_{0.13}Mn_{0.54}O_2$ was prepared by the method detailed previously.[12]

Electrochemistry. For the neutron sample, $^7Li_{1.2}Ni_{0.13}Co_{0.13}Mn_{0.54}O_2$ was intimately mixed with 10 wt% acetylene black in a pestle and mortar. Large format battery cells were employed to charge the powder mixture in loadings of 1.7-1.8 g active material (~22-23 mg cm^{-2}) at a rate of 10 mA g^{-1}. LP30 was used as the electrolyte and Li metal foil as the counter electrode. For the *ex-situ* RIXS measurements, self-supporting films were prepared by grinding the as-synthesised materials with acetylene black and polytetrafluoroethylene in an 8:1:1 mass ratio in a pestle and mortar and were subsequently calendared. Electrochemical cycling was performed in coin cells with LP30 electrolyte and a lithium metal foil counter electrode. Cells were disassembled and the electrodes rinsed with dry dimethylcarbonate.

Neutron PDF. Neutron total scattering data were collected on the POLARIS diffractometer at the ISIS Neutron Source.[34] Samples were loaded into 8mm vanadium cannisters and sealed under inert atmosphere with indium wire. For room temperature data collection, the sample can was mounted on an automatic sample changer. For data collection at 2K, the sample can was loaded into a fast cooling automatically controlled "orange" helium flow cryostat. For data reduction and PDF calculations, additional data sets were collected from an empty sample can both on the sample changer and in the cryostat, as well as a sample can filled with carbon and an empty cryostat data set. GudrunN software was used for normalisation and subtraction of the background scattering from carbon, the cannister and the cryostat.[35] Structure refinement was performed using the PDFgui front end software and PDFfit2 refinement program.[36]

Resonant Inelastic X-ray Scattering. RIXS spectra were obtained at the I21 beamline at Diamond Light Source. Samples were transferred to the spectrometer using a vacuum transfer suitcase to avoid air exposure and were pumped down to UHV and left to fully degas overnight. RIXS line scans were recorded at the resonance energy for molecular O_2 (531 eV) at fifteen different sample locations and averaged together.

Powder X-ray diffraction. PXRD patterns were obtained for the as-prepared materials using a Cu source Rigaku SmartLab diffractometer equipped with a Ge(220) double bounce monochromator and a Hypix 2D detector. Reitveld profile refinements were performed using the GSAS suite of programs. *Ex-situ* PXRD data were collected using a Rigaku miniflex benchtop diffractometer inside a glovebox under an inert atmosphere to prevent any chance of air exposure.

Operando Electrochemical Mass Spectrometry. OEMS was carried out by flowing Ar carrier gas through an ECC-std electrochemical cell (EL-CELL) with gas inlet and outlet ports and into a BT Prima mass spectrometer (Thermo Fischer). The cell contained a Li counter electrode and an electrolyte of 1M $LiPF_6$ in propylene carbonate (Merck).

Scanning Electron Microscopy and Energy Dispersive X-ray. SEM and EDX were performed using the Carl Zeiss Merlin – analytical electron microscope.

References

1. Whittingham, M. S. Ultimate Limits to Intercalation Reactions for Lithium Batteries. *Chem. Rev.* **114**, 11414–11443 (2014).

2. Koga, H. *et al.* Reversible Oxygen Participation to the Redox Processes Revealed for $Li_{1.20}Mn_{0.54}Co_{0.13}Ni_{0.13}O_2$. *J. Electrochem. Soc.* **160**, A786–A792 (2013).

3. Lu, Z. & Dahn, J. R. Understanding the Anomalous Capacity of Li/Li[$Ni_xLi_{(1/3-2x/3)}Mn_{(2/3-x/3)}$]$O_2$ Cells Using In Situ X-Ray Diffraction and Electrochemical Studies. *J. Electrochem. Soc.* **149**, A815 (2002).

4. Lu, Z., Beaulieu, L. Y., Donaberger, R. A., Thomas, C. L. & Dahn, J. R. Synthesis, Structure, and Electrochemical Behavior of Li[$Ni_xLi_{1/3-2x/3}Mn_{2/3-x/3}$]$O_2$. *J. Electrochem. Soc.* **149**, A778 (2002).

5. Oishi, M. *et al.* Direct observation of reversible oxygen anion redox reaction in Li-rich manganese oxide, Li_2MnO_3, studied by soft X-ray absorption spectroscopy. *J. Mater. Chem. A* **4**, 9293–9302 (2016).

6. Luo, K. *et al.* Charge-compensation in 3d-transition-metal-oxide intercalation cathodes through the generation of localized electron holes on oxygen. *Nat. Chem.* **8**, 684–691 (2016).

7. Seo, D.-H. *et al.* The structural and chemical origin of the oxygen redox activity in layered and cation-disordered Li-excess cathode materials. *Nat. Chem.* **8**, 692–697 (2016).

8. Saubanère, M., McCalla, E., Tarascon, J.-M. & Doublet, M.-L. The intriguing question of anionic redox in high-energy density cathodes for Li-ion batteries. *Energy Environ. Sci.* **9**, 984–991 (2016).

9. Sathiya, M. *et al.* Reversible anionic redox chemistry in high-capacity layered-oxide electrodes. *Nat. Mater.* **12**, 827–35 (2013).

10. McCalla, E. *et al.* Visualization of O-O peroxo-like dimers in high-capacity layered oxides for Li-ion batteries. *Science* **350**, 1516–21 (2015).

11. House, R. A. *et al.* Superstructure control of first-cycle voltage hysteresis in oxygen-redox cathodes. *Nature* **577**, 502–508 (2020).

12. House, R. A. *et al.* First-cycle voltage hysteresis in Li-rich 3 d cathodes associated with molecular O_2 trapped in the bulk. *Nat. Energy 2020 510* **5**, 777–785 (2020).

13. House, R. A. *et al.* Covalency does not suppress O_2 formation in 4d and 5d Li-rich O-redox cathodes. *Nat. Commun.* **12**, (2021).

14. Liu, H. *et al.* Operando Lithium Dynamics in the Li-Rich Layered Oxide Cathode Material via Neutron Diffraction. *Adv. Energy Mater.* **6**, 1502143 (2016).

15. Fell, C. R. *et al.* Correlation Between Oxygen Vacancy, Microstrain, and Cation Distribution in Lithium-Excess Layered Oxides During the First Electrochemical Cycle. *Chem. Mater.* **25**, 1621–1629 (2013).

16. Croy, J. R. *et al.* First-charge instabilities of layered-layered lithium-ion-battery materials. *Phys. Chem. Chem. Phys.* **17**, 24382–24391 (2015).

17. Grenier, A. *et al.* Nanostructure Transformation as a Signature of Oxygen Redox in Li-Rich 3d and 4d Cathodes. *J. Am. Chem. Soc.* **143**, 5763–5770 (2021).

18. Zhao, E. *et al.* Local structure adaptability through multi cations for oxygen redox accommodation in Li-Rich layered oxides. *Energy Storage Mater.* **24**, 384–393 (2020).

19. Rong, X. *et al.* Anionic Redox Reaction-Induced High-Capacity and Low-Strain Cathode with Suppressed Phase Transition. *Joule* **3**, 503–517 (2019).

20. Rong, X. *et al.* Structure-Induced Reversible Anionic Redox Activity in Na Layered Oxide Cathode. *Joule* **2**, 125–140 (2018).

21. Song, B. *et al.* A novel P3-type $Na_{2/3}Mg_{1/3}Mn_{2/3}O_2$ as high capacity sodium-ion cathode using

reversible oxygen redox. *J. Mater. Chem. A* (2019). doi:10.1039/C8TA09422E

22. Song, B. *et al.* Understanding the Low-Voltage Hysteresis of Anionic Redox in $Na_2Mn_3O_7$. *Chem. Mater.* **31**, 3756–3765 (2019).

23. Yin, W. *et al.* Structural evolution at the oxidative and reductive limits in the first electrochemical cycle of $Li_{1.2}Ni_{0.13}Mn_{0.54}Co_{0.13}O_2$. *Nat. Commun. 2020 111* **11**, 1–11 (2020).

24. Qiu, B. *et al.* Metastability and Reversibility of Anionic Redox-Based Cathode for High-Energy Rechargeable Batteries. *Cell Reports Phys. Sci.* **1**, 100028 (2020).

25. Gent, W. E. *et al.* Coupling between oxygen redox and cation migration explains unusual electrochemistry in lithium-rich layered oxides. *Nat. Commun.* **8**, (2017).

26. Tran, N. *et al.* Mechanisms Associated with the "Plateau" Observed at High Voltage for the Overlithiated $Li_{1.12}(Ni_{0.425}Mn_{0.425}Co_{0.15})_{0.88}O_2$ System. *Chem. Mater.* **20**, 4815–4825 (2008).

27. Yabuuchi, N., Yoshii, K., Myung, S.-T., Nakai, I. & Komaba, S. Detailed studies of a high-capacity electrode material for rechargeable batteries, Li_2MnO_3-$LiCo_{(1/3)}Ni_{(1/3)}Mn_{(1/3)}O_2$. *J. Am. Chem. Soc.* **133**, 4404–19 (2011).

28. Pimenta, V. *et al.* Synthesis of Li-Rich NMC: A Comprehensive Study. *Chem. Mater.* **29**, 9923–9936 (2017).

29. Leifer, N. *et al.* Linking structure to performance of $Li_{1.2}Mn_{0.54}Ni_{0.13}Co_{0.13}O_2$ (Li and Mn rich NMC) cathode materials synthesized by different methods. *Phys. Chem. Chem. Phys.* **22**, 9098–9109 (2020).

30. Menon, A. S. *et al.* Synthetic Pathway Determines the Nonequilibrium Crystallography of Li- and Mn-Rich Layered Oxide Cathode Materials. *ACS Appl. Energy Mater.* **4**, 1924–1935 (2021).

31. Zheng, J. M., Wu, X. B. & Yang, Y. A comparison of preparation method on the electrochemical performance of cathode material $Li[Li_{0.2}Mn_{0.54}Ni_{0.13}Co_{0.13}]O_2$ for lithium ion battery. *Electrochim. Acta* **56**, 3071–3078 (2011).

32. Zhao, T. *et al.* Synthesis, characterization, and electrochemistry of cathode material $Li[Li_{0.2}Co_{0.13}Ni_{0.13}Mn_{0.54}]O_2$ using organic chelating agents for lithium-ion batteries. *J. Power Sources* **228**, 206–213 (2013).

33. House, R. A. *et al.* The role of O_2 in O-redox cathodes for Li-ion batteries. *Nat. Energy 2021* 1–9 (2021). doi:10.1038/s41560-021-00780-2

34. Smith, R. I. *et al.* The upgraded Polaris powder diffractometer at the ISIS neutron source. *Rev. Sci. Instrum.* **90**, 115101 (2019).

35. Soper, A. K. *GudrunN and GudrunX: Programs for Correcting Raw Neutron and X-ray Diffraction Data to Differential Scattering Cross Section*. *RAL Report RAL-TR-2011-013* (2011).

36. Farrow, C. L. *et al.* PDFfit2 and PDFgui: computer programs for studying nanostructure in crystals. *J. Phys. Condens. Matter* **19**, 335219 (2007).

Acknowledgements

P.G.B. is indebted to the EPSRC, the Henry Royce Institute for Advanced Materials (EP/R00661X/1, EP/S019367/1, EP/R010145/1, EP/L019469/1) and the Faraday Institution (FIRG007, FIRG008) for

financial support. We acknowledge STFC for provision of ISIS Xpress Access beamtime (proposals XB1990393, 2090011 and 2090012). We acknowledge Diamond Light Source for time on I21 under proposal MM25589-1. The authors acknowledge use of characterisation facilities within the David Cockayne Centre for Electron Microscopy, Department of Materials, University of Oxford, alongside financial support provided by the Henry Royce Institute (EP/R010145/1).

Author Contributions

R.A.H. planned and conducted the synthesis and characterisation work. H.Y.P. and R.I.S. collected the neutron total scattering data and performed data reduction. R.A.H. performed the PDF fitting. J.H. and I.G. planned and performed the electron microscopy work. R.A.H. and K.Z. conducted the RIXS measurements. R.A.H. and P.G.B. wrote the manuscript with contributions from all authors.

Competing Interest Statement

The authors declare no competing interests.

Data Availability Statement

Supporting research data is available under the following DOIs:
https://doi.org/10.5286/ISIS.E.RB2090011-1, https://doi.org/10.5286/ISIS.E.RB2090012-1,
https://doi.org/10.5286/ISIS.E.RB1990393-1

Supplementary Information

Detection of trapped molecular O_2 in a charged Li-rich cathode by Neutron PDF

Robert A. House, Helen Y. Playford, Ronald I. Smith, Jennifer Holter, Ian Griffiths, Ke-Jin Zhou, Peter G. Bruce

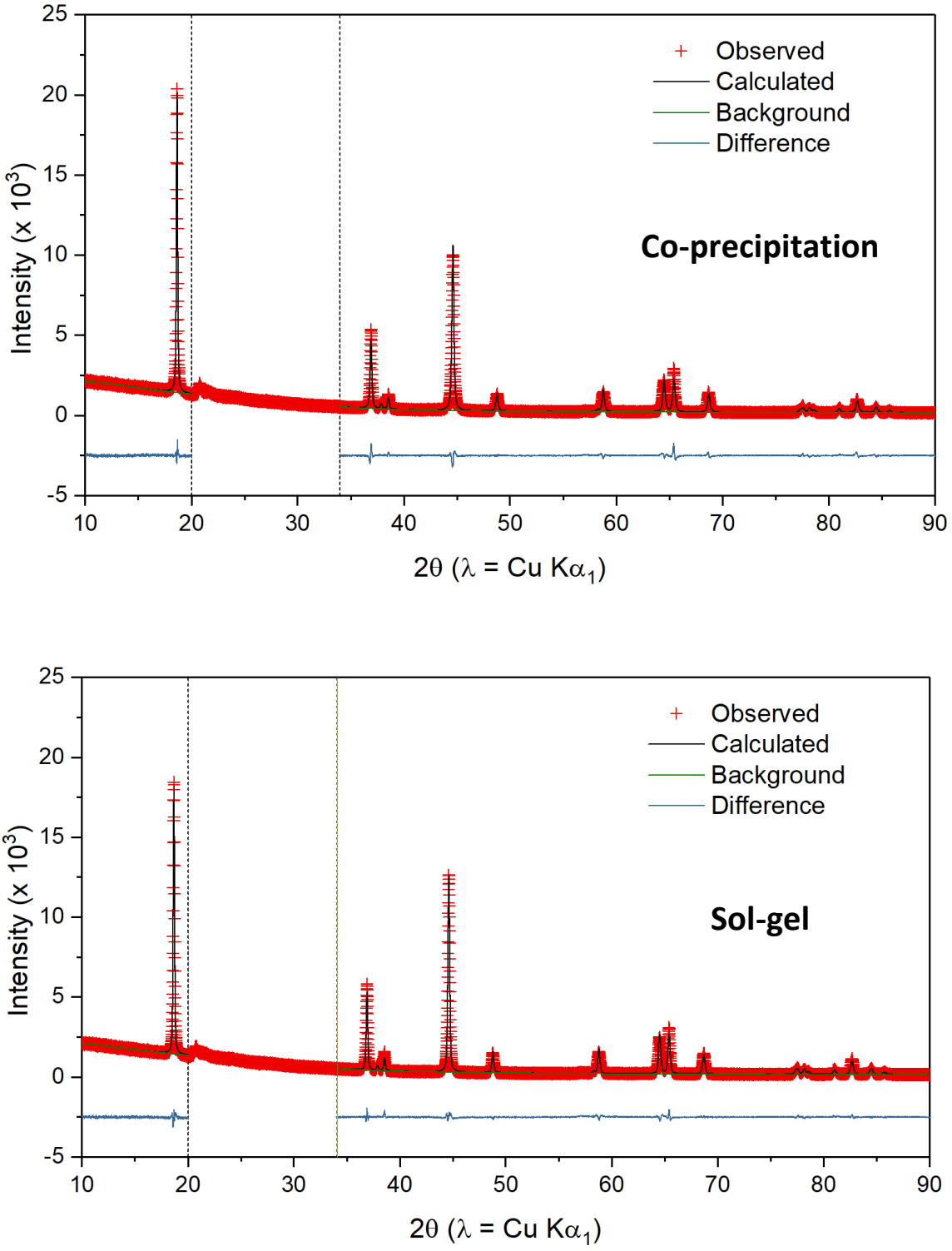

Supp. Fig. 1. Fitted PXRD data following Rietveld refinement for pristine $Li_{1.2}Ni_{0.13}Co_{0.13}Mn_{0.54}O_2$ prepared by carbonate co-precipitation (upper panel) and sol-gel (lower panel).

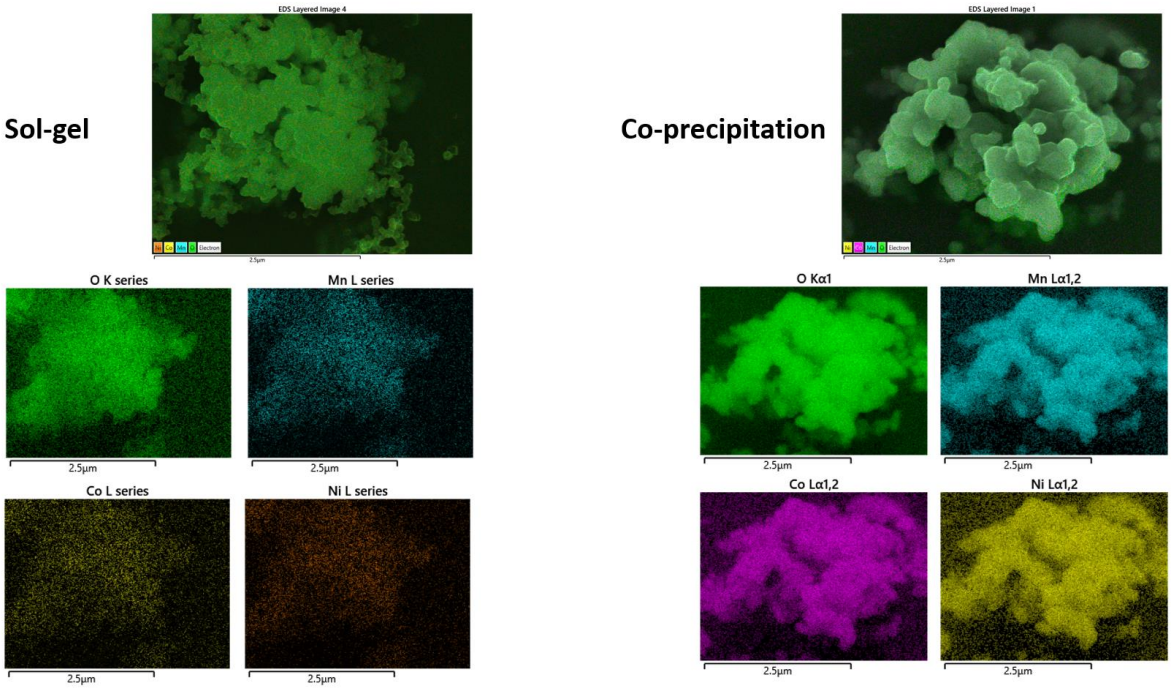

Supp. Fig. 2. EDX images. Homogeneous mixing of transition metals within and between primary particles for pristine $Li_{1.2}Ni_{0.13}Co_{0.13}Mn_{0.54}O_2$ prepared by sol-gel and carbonate co-precipitation.

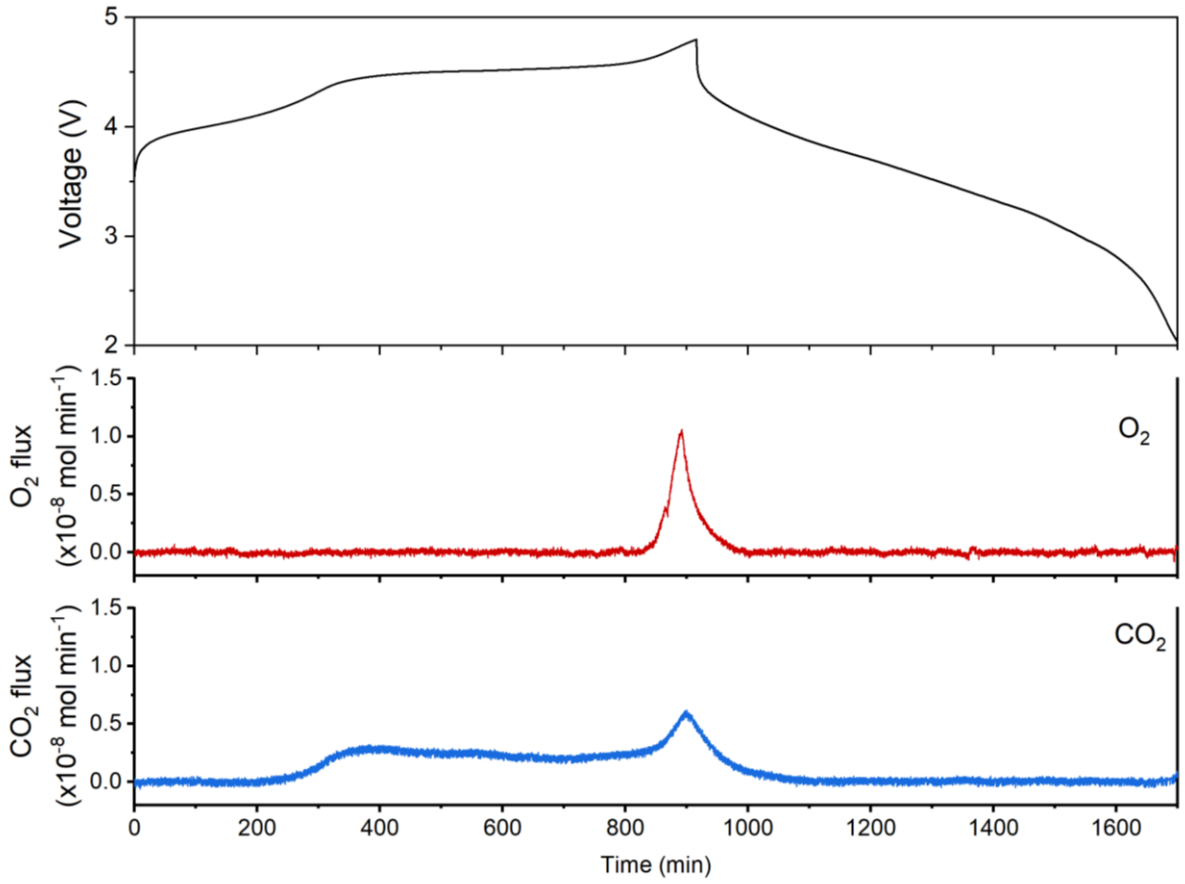

Supp. Fig. 3. OEMS data. Evolved O_2 and CO_2 gases detected by mass spec for co-precipitation derived $Li_{1.2}Ni_{0.13}Co_{0.13}Mn_{0.54}O_2$ charged at a rate of 20 mA g^{-1} between 2 and 4.8 V. 0.0041 moles of O_2 and 0.0159 moles of CO_2 were evolved per mole of $Li_{1.2}Ni_{0.13}Co_{0.13}Mn_{0.54}O_2$ during the first cycle. The electrode active material mass for the experiment was 10.32 mg.

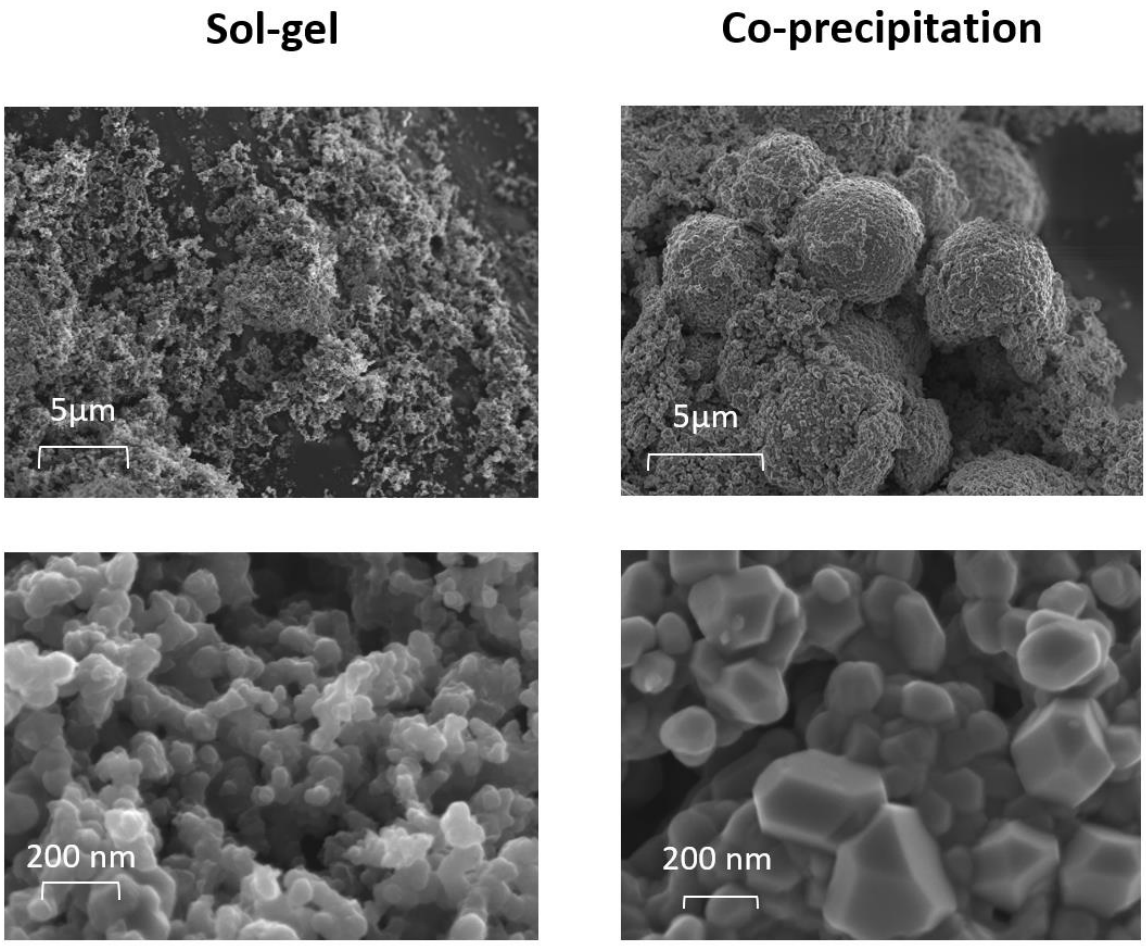

Supp. Fig. 4. SEM images Primary and secondary particle morphology for pristine $Li_{1.2}Ni_{0.13}Co_{0.13}Mn_{0.54}O_2$ prepared by sol-gel and carbonate co-precipitation.

Supp. Tab. 1. X-ray diffraction refinement parameters for **a** pristine $^{7}Li_{1.2}Ni_{0.13}Co_{0.13}Mn_{0.54}O_2$ prepared by co-precipitation for the neutron study and **b** $Li_{1.2}Ni_{0.13}Co_{0.13}Mn_{0.54}O_2$ prepared by sol-gel.

a

Atom	Wycoff	x	y	z	Occupancy	U_{iso}
^{7}Li	3a	0	0	0	1	0.0137(2)
Li/Ni/Co/Mn	3b	0	0	0.5	0.2/0.13/0.13/0.54	0.0140(4)
O	6c	0	0	0.2405(1)	1	0.0243(5)
S.G. = R-3m R_w = 0.0555 G.O.F. = 1.6			a = 2.849(1) Å c = 14.226(1) Å		α = 90 β = 90 γ = 120	

b

Atom	Wycoff	x	y	z	Occupancy	U_{iso}
^{7}Li	3a	0	0	0	1	0.0135(2)
Li/Ni/Co/Mn	3b	0	0	0.5	0.2/0.13/0.13/0.54	0.0126(3)
O	6c	0	0	0.2416(1)	1	0.0201(4)
S.G. = R-3m R_w = 0.0516 G.O.F. = 1.5			a = 2.850(1) Å c = 14.221(1) Å		α = 90 β = 90 γ = 120	

Supp. Tab. 2. Neutron PDF refinement parameters for pristine $^{7}Li_{1.2}Ni_{0.13}Co_{0.13}Mn_{0.54}O_2$

Atom	Wycoff	x	y	z	Occupancy
^{7}Li	4h	0	0.3328(7)	0.5	1
^{7}Li	2c	0	0	0.5	1
^{7}Li/Ni	2b	0	0.5	0	0.6/0.4
Co/Mn	4g	0	0.1617(8)	0	0.2/0.8
O	8j	0.2511(6)	0.3222(2)	0.2231(3)	1
O	4i	0.2184(7)	0	0.2256(5)	1
S.G. = C2/m, R_w = 0.092, Q_{max} = 30 Å, r = 0.5 – 40 Å		a = 4.942(1) Å b = 8.547(2) Å c = 5.031(1) Å		α = 90 β = 109.33(2) γ = 90	

Supp. Tab. 3. X-ray refinement parameters for 4.8V charged $^{7}Li_{0.1}Ni_{0.13}Co_{0.13}Mn_{0.54}O_2$

Atom	Wycoff	x	y	z	Occupancy	U_{iso}
^{7}Li/Ni	4h	0	0.333	0.5	0.1/0.03	0.0094(7)
^{7}Li/Ni	2c	0	0	0.5	0.1/0.03	0.0094(7)
Ni/Co/Mn	2b	0	0.5	0	0.10/0.13/0.54	0.0094(7)
Ni/Co/Mn	4g	0	0.167	0	0.10/0.13/0.54	0.0094(7)
O	8j	0.251(5)	0.335(2)	0.235(6)	1	0.0094(7)
O	4i	0.235(1)	0	0.246(1)	1	0.0094(7)
S.G. = C2/m			a = 4.912(2) Å		α = 90	
R_w = 0.0252			b = 8.493(1) Å		β = 108.94(1)	
G.O.F. = 1.2			c = 4.948(2) Å		γ = 90	

Supp. Tab. 4. Neutron PDF refinement parameters for 4.8V charged $^{7}Li_{0.1}Ni_{0.13}Co_{0.13}Mn_{0.54}O_2$

Atom	Wycoff	x	y	z	Occupancy
^{7}Li	4h	0	0.333	0.5	0.1
^{7}Li	2c	0	0	0.5	0.1
Ni/Co/Mn	2b	0	0.5	0	0.13/0.13/0.54
Ni/Co/Mn	4g	0	0.167	0	0.13/0.13/0.54
O	8j	0.246(2)	0.337(1)	0.227(1)	1
O	4i	0.237(1)	0	0.200(2)	1
S.G. = C2/m, R_w = 0.193, Q_{max} = 26 Å, r = 0.5 – 40 Å		a = 4.919(4) Å b = 8.486(8) Å c = 4.975(3) Å		α = 90 β = 109.97(6) γ = 90	

Supp. Tab. 5. Neutron PDF refinement parameters for 4.8V charged $^{7}Li_{0.1}Ni_{0.13}Co_{0.13}Mn_{0.54}O_2$ **a** without and **b** with Ni migration.

a

Atom	Wycoff	x	y	z	Occupancy
^{7}Li	4h	0	0.333	0.5	0.1
^{7}Li	2c	0	0	0.5	0.1
Ni/Co/Mn	2b	0	0.5	0	0.13/0.13/0.54
Ni/Co/Mn	4g	0	0.167	0	0.13/0.13/0.54
O	8j	0.250(2)	0.330(3)	0.214(5)	1
O	4i	0.256(3)	0	0.201(9)	1
S.G. = C2/m R_w = 0.193, Q_{max} = 26 Å r = 0.5 – 4 Å		a = 5.02(3) Å b = 8.28 (4) Å c = 5.04(3) Å		α = 90 β = 111.9(4) γ = 90	

b

Atom	Wycoff	x	y	z	Occupancy
^{7}Li/Ni	4h	0	0.333	0.5	0.1/0.031(7)
^{7}Li/Ni	2c	0	0	0.5	0.1/0.031(7)
Ni/Co/Mn	2b	0	0.5	0	0.099(7)/0.13/0.54
Ni/Co/Mn	4g	0	0.167	0	0.099(7)/0.13/0.54
O	8j	0.250(2)	0.329(2)	0.214(4)	1
O	4i	0.256(3)	0	0.200(8)	1
S.G. = C2/m R_w = 0.166, Q_{max} = 26 Å r = 0.5 – 4 Å		a = 5.01(5) Å b = 8.28 (7) Å c = 5.04(3) Å		α = 90 β = 111.7(5) γ = 90	

Supp. Tab. 6. Neutron PDF refinement parameters for 4.8V charged $^{7}Li_{0.1}Ni_{0.13}Co_{0.13}Mn_{0.54}O_2$ with Ni migration and solid beta-O_2 phase.

$^{7}Li_{0.1}Ni_{0.13}Co_{0.13}Mn_{0.54}O_2$ phase fraction = 0.34

Atom	Wycoff	x	y	z	Occupancy
^{7}Li/Ni	4h	0	0.333	0.5	0.1/0.031
^{7}Li/Ni	2c	0	0	0.5	0.1/0.031
Ni/Co/Mn	2b	0	0.5	0	0.099/0.13/0.54
Ni/Co/Mn	4g	0	0.167	0	0.099/0.13/0.54
O	8j	0.250	0.329	0.214	1
O	4i	0.256	0	0.200	1
S.G. = C2/m R_w = 0.138, Q_{max} = 26 Å r = 0.5 – 4 Å		a = 5.01 Å b = 8.28 Å c = 5.04 Å			α = 90 β = 111.7 γ = 90

Beta-O_2 phase fraction = 0.66

Atom	Wycoff	x	y	z	Occupancy
O	6c	0	0	0.0536	1
S.G. = R-3m R_w = 0.138, Q_{max} = 26 Å r = 0.5 – 4 Å		a = 3.307 Å b = 3.307 Å c = 11.26 Å			α = 90 β = 90 γ = 120

Spherical particle diameter (spdiameter = 3.6(8) Å) was also refined to reduce the contribution of intermolecular correlations to the PDF.